Available online at www.sciencedirect.com
SCIENCE DIRECT®
Thermochimica Acta 432 (2005) 186–191
thermochimica acta
www.elsevier.com/locate/tca

Nanocalorimeter fabrication procedure and data analysis for investigations on implantation damage annealing

R. Karmouch*, J.-F. Mercure, F. Schiettekatte

Regroupement Québécois sur les Matériaux de Pointe (RQMP), Département de physique, Université de Montréal, C.P. 6128 succ. centre-ville, Montréal, Qué., Canada H3C 3J7

Received 31 August 2004; received in revised form 10 December 2004; accepted 22 December 2004
Available online 26 January 2005

Abstract

Nanocalorimetry operates on similar principles as conventional differential thermal analysis, but the thinness of the system provides a mass addenda small enough to observe thermal processes in thin films or at surface, involving energies in the order of the nanojoules. The fabrication procedure of nanocalorimeters used to measure the heat released by damage after low-energy (30 keV) ion implantation in polycrystalline silicon (poly-Si) is described. Nanocalorimeters are fabricated from low-stress Si_3N_x membranes (100 nm) on which a Pt strip (25 nm) is deposited which serves both as a heater and thermometer. Using Pt allows us to carry out the metallization step prior to Si anisotropic chemical etching releasing the rectangular Si_3N_x membrane, so the success yield nearly reaches 100%. A 140 nm Si layer is deposited on the nanocalorimeters. Large-grain (∼75 nm) poly-Si is obtained by annealing at 900 °C for 100 s. The calculation method used to obtain heat rate curves is described, including the corrections necessary to take into account the dissimilarity between sample and reference calorimeters (baseline), and the increased heating rate and associated losses. Examples of heat release after 30 keV Si implantations are presented, showing that the total amount of heat release is characterized by a saturation above a fluence of 1 Si^-/nm^2. The similarity observed in the signal shape between low and high fluence measurements also suggests that each impacting ion produces a high damage zone similar to the damage generated by high fluence irradiation. This conclusion is compatible with the annealing of damage zones proposed by molecular dynamic studies. It is also shown that the measured signal is not affected significantly by temperature non-uniformity.
© 2004 Elsevier B.V. All rights reserved.

Keywords: Nanocalorimetry; Silicon nitride membranes; Ion implantation; Damage annealing

1. Introduction

Ion implantation produces considerable lattice damage due to the energetic collisions of ions with lattice atoms. In monocrystalline silicon, defect complexes stable at room temperature (RT) dissociate upon annealing, releasing interstitials and vacancies. Most of them will eventually recombine quickly until only interstitials remain in the sample, their amount being roughly equal to the number of implanted ions. These excess interstitials drive several phenomena such as the transient enhanced diffusion (TED) [1] namely through {3 1 1} rod-like defect coarsening [2,3]. Since the TED enhancement and duration depend on the thermal stability of defects storing the interstitials, it is fundamental to characterize their thermal evolution. While there are detailed experimental and theoretical studies on extended defects [4], the cluster phase evolution of defect below 680 °C still requires experimental data to compare to proposed models. Spectrometric methods [5,6] will only be able to probe certain types of electrically active defects, while ion implantation generates complex defect structures that may not be observable by such techniques.

A different approach to the problem is to use calorimetric methods to look at damage annealing from the thermal

* Corresponding author. Tel.: +1 514 343 6111 4209; fax: +1 514 343 6215.
E-mail address: rachid.karmouch@umontreal.ca (R. Karmouch).

0040-6031/$ – see front matter © 2004 Elsevier B.V. All rights reserved.
doi:10.1016/j.tca.2004.12.014

point view, i.e. to measure the amount of heat required or given off by such process. These techniques provide information on energy activation and heat exchange during all thermal processes occurring in a sample. In the last decade, researchers have used conventional differential scanning calorimeter (DSC) to investigate high-energy proton irradiated in silicon [7] and self-implanted amorphous silicon (a-Si) relaxation [8,9]. However, this technique is not sensitive enough to look at the annealing of low-energy (<100 keV) implanted defects, since the power required to heat the calorimetric cell itself is orders of magnitude larger than the power released by the defects. The signal would thus be lost in the addenda.

The advances in micro-electromechanical systems fabrication techniques, using silicon nitride membranes makes possible the fabrication of calorimetric devices with low thermal mass [10] that combine the four components found in calorimetry in a single multilayer thin film system, namely: the sample, a sample holder, a thermometer and a heater. This technique allowed us to measure in situ the heat released by damage annealing following low-energy (≤30 keV) ion implantation in polycrystalline silicon (poly-Si). In this paper, we report our nanocalorimeter fabrication procedure, and a summary of the calculation steps and corrections required by the data analysis. The issue of temperature non-uniformity across the deposited sample is also addressed.

2. Nanocalorimeter device fabrication

The processing steps to prepare the nanocalorimeters are represented schematically in Fig. 1. We start with a (1 0 0) oriented silicon wafer, polished on both sides. A thin (100 nm), high density, low-stress silicon nitride layer (200 MPa tensile stress; refractive index 2.2) is deposited on both sides of the wafer by means of Si-rich low-pressure chemical vapor deposition (LPCVD, Fig. 1a).

One side of the wafer is patterned using two different positive photoresist. The first one (Microchem LOR-5A) is spin-

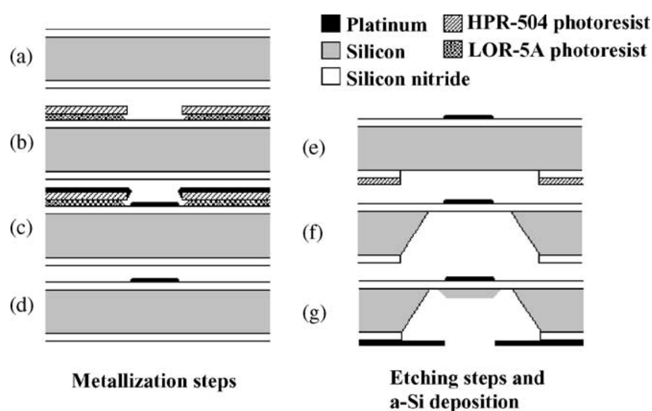

Fig. 1. Cross-section of the nanocalorimeter device at different steps of fabrication.

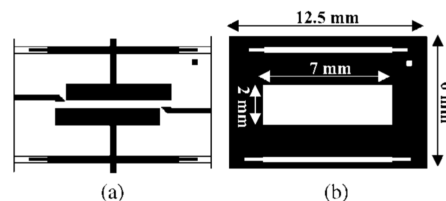

Fig. 2. (a) Metallization mask: metallic strip width is 0.5 mm and (b) etching mask: white parts are the exposed surfaces. The small square in upper right corner is a marker for alignment using the infrared camera.

coated at 2800 rpm during 35 s and soft-baked at 140 °C for 3 min. The second one (Olin Microelectronic Materials HPR-504) is spin-coated at 3000 rpm, followed by a soft-bake at 130 °C for 60 s. Using LOR-5A in combination with a conventional positive resists such as HPR-504 allows us to control the amount and rate of undercut [11], making the lift-off operation easier after metal deposition. After an exposition of the wafer to UV-light for 25 s (140 mJ/cm^2) using the metallization mask (Fig. 2a), we develop the second photoresist for 35 s and then the first one for 45 s in the same developer (Fig. 1b).

In the next step, a 3 nm titanium adhesion layer is deposited by evaporation, followed by the deposition of 25 nm of platinum by Ar sputtering (Fig. 1c). The choice of platinum is based on the favorable qualities of this metal. It does not oxidize; its resistance versus temperature is fairly linear over a broad temperature range (100–1200 K); it is a non-ferromagnetic metal; it is chemically strong enough to withstand exposition to tetramethylammonium hydroxide (TMAH) for a few hours.

Once the metal deposition step is finished, we perform a lift-off by soaking the wafers in acetone for 10 min followed by 1 min in the remover of the first photoresist. During the lift-off, the wafer must be vertically tilted and a dropper is used to spray gently on the wafer. The solvent should not be stirred too much in order to avoid that metal pieces stick back on the wafer, letting parts of the wafer unexposed to acetone during the process. After the lift-off, the wafers are thoroughly cleaned with acetone to remove any remaining pieces of metal. This operation lasts the metallization step for the front side (Fig. 1d). The backside is then patterned using only one photoresist (HPR-504) spin-coated at 3000 rpm for 35 s and soft-baked at 130 °C for 60 s. The etching mask (Fig. 2b) is then aligned using alignment marks that were patterned on the front side. For this purpose, we use an IR camera on the backside, shining ordinary light from the metallization side (Fig. 2a). The backside is then exposed to UV-light (140 mJ/cm^2) for 25 s. After a 35 s development, the photoresist is hard-baked at 130 °C for 3 min to increase adhesion and to make it harder for subsequent steps. The exposed silicon nitride is then removed by reactive ion etching using a plasma of SF_6 (13 sccm) and He (7 sccm). The etching rate is 100 nm/min with a uniformity of 5% and selectivity of 0.8 to photoresist and 0.33 to silicon (Fig. 1e).

The last step consists in etching anisotropically the silicon in areas where the Si_3N_x masking layer is removed using a TMAH solution (25%, w/w) at 90 °C, providing an etching rate of around 50 μm/h (Fig. 1f). About 6–8 h are required to remove completely the silicon. The silicon nitride membrane becomes a 7 mm × 2 mm window at the center of 12.5 mm × 6 mm rectangular silicon frame. With these dimensions, we are able to fit eight devices per square inch. This fabrication procedure allows us to reach a success yield of nearly 100% compared to a method where the metallization is carried out at the end, on free membranes, with, in our case, a yield around 50%. It presents one drawback related to the metal choice that is limited to platinum. This heavy metal may for instance dominate the signal when performing transmission electron microscopy (TEM) directly on the nanocalorimeters.

At this point, we get virgin nanocalorimeters such as those that have been developed by Allen and co-workers to investigate the melting point depression in nanostructures [10,12,13], and the glass transition in thin polymer films [14]. We now apply it to the damage annealing in implanted poly-Si and the relaxation of self-implanted a-Si [15,16].

3. Sample deposition and principle of operation

For our implantation experiments, a 140 nm a-Si layer is deposited by sputtering in an Ar environment, on the opposite side of the membrane using a shadow mask (Fig. 1g). Its width is effectively 650 μm, that is, it exceeds the heater strip width by ∼75 μm from each side. The question of the excess width of the Si layer with respect to the width of the Pt heater and corresponding temperature uniformity is addressed in Section 6. Its length extends past each contact point (Fig. 2a). The membrane is thin enough to ensure a good thermal conduction between the sample and the heater, while it isolates them electrically. For damage annealing investigations in implanted poly-Si, the nanocalorimeters were annealed at 900 °C during 100 s in a N_2 atmosphere to form a poly-Si layer with crystallites of ∼75 nm.

Each nanocalorimetry experiment is preceded by the Pt resistance calibration. The nanocalorimeters are placed in a furnace under N_2 atmosphere at 450 °C and the temperature is slowly decreased down to RT while recording the Pt resistance $R(T)$. The data are well modelled by the following expression:

$$R(T) = R_0(1 + \beta_R T + \gamma_R T^2) + R_1 \quad (1)$$

where T is the temperature expressed in °C, $R_0 + R_1$ the resistance at 0 °C, and β_R and γ_R the linear and quadratic coefficients of the resistance temperature dependence of Pt, respectively, $3.9083 \times 10^{-3}\,K^{-1}$ and $-5.8019 \times 10^{-7}\,K^{-2}$. Ref. [17] indicates that such a quadratic dependence is valid up to 1000 °C, so $R(T)$ could be extrapolated to carry out measurements at higher temperatures. Here, we only present the results in the temperature range of the calibration without extrapolation. The resistance is typically 70 Ω and varies by a maximum of 2 Ω for a batch of nanocalorimeters fabricated on the same wafer. Different batches, deposited at different times, may vary by 10–20 Ω.

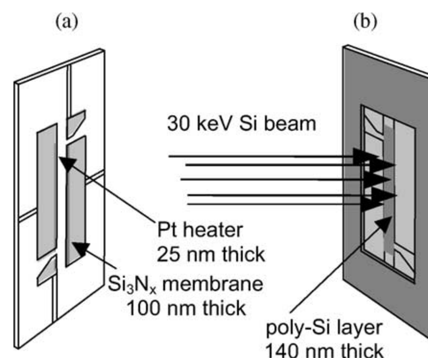

Fig. 3. Calorimeter view from: (a) the front side and (b) backside. The 140 nm of poly-Si is deposited on Si_3N_x from the backside in line with the Pt strip. The implantation is carried from the backside on one nanocalorimeter, the other serving as a reference.

The heat release measurements are then performed in differential mode. Two almost identical nanocalorimeters, both with a poly-Si layer deposited on their membrane and selected on the basis of to their $R(T)$ calibration, are placed side by side in the implantation chamber, one of them being implanted in order to induce damage while the other serves as a reference and remains unimplanted (Fig. 3). A calorimetry measurement is initiated by supplying a ∼25 mA, 25 ms current pulse to the Pt heater, thus raising the temperature of the system by Joule heating. The current I and voltage V are monitored in real time during the pulse (using IoTech 488 analog–digital converters), so the heat supplied to the system is directly obtained ($P = VI$). The temperature of the system is determined by computing the resistance of the Pt heater ($R = V/I$), and then using the calibration of the resistance as a function of the temperature established beforehand.

4. Data analysis

Nanocalorimetry measurements are presented in terms of heat rate, that is, the amount of heat per unit degree generated by damage annealing. In order to determine the heat rate, we use the method developed by Efremov et al. to calculate the heat capacity of a deposited layer [18]. Here, however, both the implanted and reference nanocalorimeters have poly-Si deposited on then, so heat capacity does not contribute to the net signal; only damage annealing does. This section summarises the calculation steps in order to explain each correction.

Starting with two nominally identical nanocalorimeters, the amount of heat per unit degrees transferred to a process occurring on the implanted (imp) nanocalorimeter compared

to the reference (ref) is given by:

$$q = (VI/\nu)_{\rm imp} - (VI/\nu)_{\rm ref} \qquad (2)$$

where ν is the heating rate ($\sim 4\times 10^4$ K/s). The effects of damage annealing, by releasing heat to the implanted nanocalorimeter is to increase slightly its heating rate. A released heat thus corresponds to a negative q value. The results presented here show rates of heat released, thus $-q$.

By directly measuring differential voltage $\Delta V = V_{\rm imp} - V_{\rm ref}$ (using an Agilent 3458A analog–digital converter), sensitivity can be drastically improved [19]. Eq. (2) can be rewritten:

$$q = \frac{(VI)_{\rm imp}}{\nu_{\rm ref}(\nu_{\rm imp}/\nu_{\rm ref})}\left[1 - \frac{\nu_{\rm imp}}{\nu_{\rm ref}}\left(1 - \frac{\Delta V}{V_{\rm imp}}\right)\frac{I_{\rm ref}}{I_{\rm imp}}\right] \qquad (3)$$

In Eq. (3), the noisy component, $\nu_{\rm imp}/\nu_{\rm ref}$, is isolated. This noise can be significantly reduced using ΔV and information on the circuit providing the current pulse [18].

The end results also include a number of corrections. First, in Eq. (3), the reference and sample calorimeters are supposed identical. A slight difference always exists, and pre-implantation measurements are carried out to estimate this baseline:

$$q_0 = (VI/\nu)^0_{\rm imp} - (VI/\nu)^0_{\rm ref} \qquad (4)$$

where 0 refers to baseline measurements. (This equation can also be rewritten in the same form as Eq. (3)). Subtracting q_0 from q obtained after an ion implantation experiment gives:

$$q_1 = q(t_i) - q_0(t_i) \qquad (5)$$

where t_i is a discrete measurement time.

It is worth noting that as long as the reference is not altered, this correction actually cancels out from Eq. (2) the term related to the reference. The role of the reference is thus essentially to match the sample calorimeter in order to provide a ΔV as small as possible, so it can be amplified. Its heating rate, $\nu_{\rm ref}$ is also important in Eq. (3), but does not change during a series of measurements and can be averaged from arbitrarily large number of scans to improve its precision.

Then, Eq. (5) is calculated at same time intervals t_i rather than at same temperature T. This is required if one wants to use ΔV in the process. As heat released by damage slightly accelerates implanted nanocalorimeter heating, this introduces an error in the calculation since $T_{\rm imp}(t_i) \neq T^0_{\rm imp}(t_i)$. While q_0 is known only for temperatures $T^0_{\rm imp}(t_i)$ it can be evaluated at temperatures $T_{\rm imp}(t_i)$ by carrying out the following calculation:

$$q_0(T_{\rm imp}(t_i)) = q_0(T^0_{\rm imp}(t_i)) - \left.\frac{\partial q_0(T^0_{\rm imp})}{\partial T_{\rm imp}}\right|_{T=T^0_{\rm imp}(t_i)} \times (T_{\rm imp}(t_i) - T^0_{\rm imp}(t_i)) \qquad (6)$$

The heat rate then becomes:

$$q_2(T_{\rm imp}) = q_1(T_{\rm imp}) - q_0(T_{\rm imp}) \qquad (7)$$

Finally, the slight change in sample calorimeter heating rate will also change the amount of thermal losses that it undergoes during a scan compared to the baseline. The losses are essentially radiative and increase as T^4. While these losses are small because of the high heating rate, they still need to be considered at high temperatures. Using a procedure described in Ref. [18], the power of heat losses $P_{\rm HL}(T)$ can be estimated using baseline measurements at different heating rates, and the associated correction becomes:

$$q_{\rm HL} = P_{\rm HL}(T_{\rm imp})\left(\frac{1}{\nu_{\rm imp}} - \frac{1}{\nu^0_{\rm imp}}\right) \qquad (8)$$

The heat flow with all the three corrections is:

$$q_3(T_{\rm imp}) = q_2(T_{\rm imp}) - q_{\rm HL}(T_{\rm imp}) \qquad (9)$$

The validity of this calculation method has been thoroughly tested for several artificially generated signal shapes, confirming that it precisely gives back the actual amount of heat released [20].

5. Implantation experiments

Low-energy 30 keV Si^- implants were performed by extracting negatively charged ions from a sputtering source biased at the desired voltage, without net acceleration inside a Tandetron accelerator. The implantations were carried out at RT, at fluences ranging from 0.001 to 8 Si^-/nm^2. According to SRIM 2003 simulations [21], the projected range is 73 nm. No ions could reach the Si_3N_x membrane or the Pt heating strip and are all stopped within the poly-Si layer. This is confirmed by the fact that the calibration $R(T)$ is not altered by the implantations, as it would be the case if the Pt strip is implanted.

Each implantation was followed by 10 nanocalorimetry scans. During each scan, the nanocalorimeters heat up above 700 °C, which should be sufficient to anneal any remaining defects. No measurable amount of heat was released after the first scan (Fig. 4), the signals of scans 2–10 falling back exactly on the baseline obtained prior to implantations.

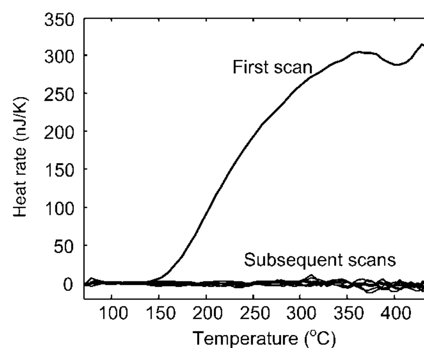

Fig. 4. Rate of heat release during a series of 10 scans following a 30 keV Si^- implantation at a fluence 8 ions/nm^2.

6. Heat release and temperature uniformity

Fig. 5(a) shows the heat release rate as a function of temperature after Si implantations at different fluences normalized by the poly-Si width. The heat release shows a broad, featureless temperature dependence. No peaks are observed in the heat rate curves that can be related to isolated kinetic processes. This shape can rather be associated to a continuous spectrum of activation energies. The released heat increases monotonically with fluences but not linearly. In Fig. 6 , where the total heat release is computed by integrating the area under each curve between 100 and 400 °C, it is seen that the signal starts to saturate around a fluence of 1 Si^{-}/nm^2, suggesting that if further transformations occur in the materials, it is not at the expense of more stored energy.

One important aspect revealed by these measurements is that the shape of the signal is similar from low to high fluences. The signal similarity suggests that the annealing kinetics of damage produced by sparse collision cascades results in a heat release that is not different from that of highly damaged Si. The signal similarity of damage annealing in poly-Si can thus be described as a process internal to the damage zone induced by each ion, as discussed in details in Ref. [15]. This explanation complies with molecular dynamics simulations [22,23] and other experiments [24] that show how the annealing of damage zones primarily depends on the details of the damage-crystal interface, rather than on the defect concentration.

Finally, another issue that has to be addressed is the influence of the temperature uniformity on the signal. A good indication of the temperature uniformity on the nanocalorimeter membrane itself (without poly-Si) is actually provided by the width of a melting peak. Fig. 5(b) shows the melting peak obtained for a 20 nm Sn layer.

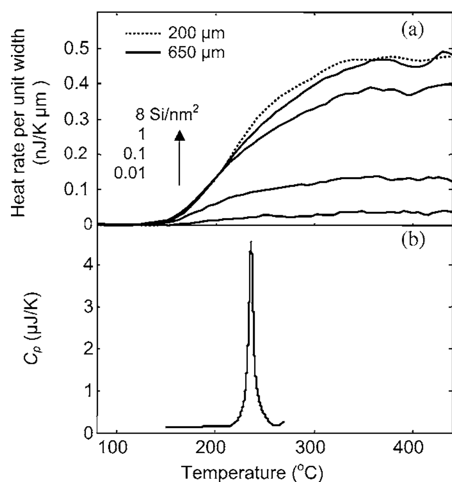

Fig. 5. (a) Rate of heat release by poly-Si implanted at indicated fluences without slit (solid lines) and, for the highest fluence, through a 200 μm slit aligned to the center of the heating strip(dashed line) and (b) melting peak of a 20 nm Sn layer.

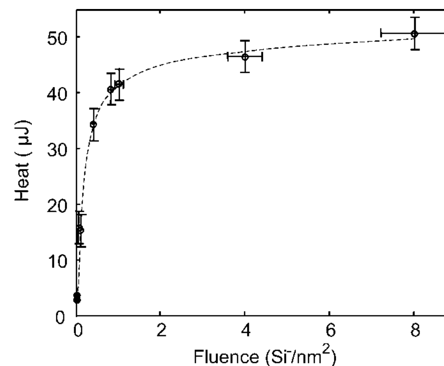

Fig. 6. Total heat release between 100 and 400 °C by implanted poly-Si as a function of fluence.

Considering that the peak may be slightly broadened by melting point depression effects [12], its width thus gives an upper limit of about 5 °C at 240 °C on the temperature non-uniformity [25]. In these experiments, the poly-Si layer was somewhat wider than the heating strip. In order to calculate this influence, we carried out one-dimensional (1D) finite differences simulations of our system, considering the cross-section of the heating strip and the membrane. 1D simulations are acceptable in this case as the length of the heating strip is 14 times longer than its width [26]. Considering that the heat conductivity of poly-Si is an order of magnitude lower than for monocrystalline Si [27], these simulations indicate that the temperature uniformity is always better than 10%, that is, 6 °C at 100 °C, and 28 °C at 300 °C. Still, in order to verify experimentally how temperature uniformity did affect our signal, we carried out measurements using an implantation slit of 200 μm in width, carefully aligned with the central axis of the heating strip. Temperature uniformity within this region should be better than 3 °C at 300 °C. As material located outside the region exposed through the slit remains unimplanted, it will not contribute any net signal after baseline subtraction. The resulting curve is plotted in Fig. 5(a) (dashed line). It is seen that the signal is slightly higher at the end of the initial rise. This is expected as the central region of the heating strip has a slightly higher temperature than the sides [25], releasing heat earlier in the scan. Our temperature measurement, which is the average over the heating strip, thus underestimates the temperature of the region implanted with a slit. The ideal signal (with a perfectly uniform temperature) should be closer to the one obtained after implantations without slits, as the temperature of the implanted region is, on average, the temperature of the heating strip.

But most importantly, the curve obtained with slits does not differ significantly from the data obtained without implantation slit, neither reveals it any new feature that could have been washed out by temperature non-uniformity. We can thus consider that the measurements carried out without slits reflect the actual shape and intensity of the signal.

7. Conclusion

In conclusion, we presented a reliable method for nanocalorimetry device fabrication, in which Si_3N_x windows opening is carried out after metallization. We also demonstrated our ability to use nanocalorimetry to investigate the kinetics of damage annealing following low-energy ion implantation. This requires the application of a calculation method that takes into accounts slight dissimilarities between sample and reference nanocalorimeters, sample nanocalorimeter increased heating rate due to damage heat release, and associated increased heat losses. It is also shown that the influence of the temperature non-uniformity on the signal is relatively limited. The released heat measurements reveal that the shape of the heat rate signal is similar over a broad fluence range, strongly suggesting that the annealing process can be described as a process internal to the damage zone of each ion.

Acknowledgments

The authors are grateful to L.H. Allen, M. Zhang and M.Yu. Efremov (UIUC), and to S. Roorda and M. Chicoine (Université de Montréal) for fruitful discussions. Thanks also go to L. Godbout, R. Gosselin for their excellent technical assistance with the accelerator operation, Y.Q. Wang for TEM, and M. Skvarla and P. Infante of the Cornell Nanofabrication Facility, as well as M.-H. Bernier and S. Bah of the École Polytechnique de Montréal for their assistance with nanocalorimeters fabrication. This work benefited from the financial support of NanoQuébec, the Fonds Québécois de Recherche sur la Nature et les Technologies and the Natural Science and Engineering Research Council of Canada.

References

[1] R.J. Schreutelkamp, J.S. Custer, J.R. Liefting, W.X. Lu, F.W. Saris, Mater. Sci. Rep. 6 (1991) 275.
[2] S. Libertino, S. Coffa, J.L. Benton, Phys. Rev. B 63 (2001) 195206.
[3] J. Kim, F. Kirchhoff, J.W. Wilkins, F.S. Khan, Phys. Rev. Lett. 84 (3) (2000) 503.
[4] B. Colombeau, N.E.B. Cowern, F. Cristiano, P. Calvo, N. Cherkashin, Y. Lamrani, A. Claverie, Appl. Phys. Lett. 83 (2003) 1953.
[5] N.E.B. Cowern, G. Mannino, P.A. Stolk, F. Rooseboom, H.G.A. Huizing, J.G.M. van Berkum, F. Cristiano, A. Claverie, M. Jaraiz, Phys. Rev. Lett. 82 (1999) 4460.
[6] S. Libertino, J.L. Benton, D.C. Jacobson, D.J. Eaglesham, J.M. Poate, S. Coffa, P. Kringhøj, P.G. Fuochi, M. Lavalle, Appl. Phys. Lett. 71 (1997) 389.
[7] R. Poirier, S. Roorda, F. Schiettekatte, M. Lalancette, J. Zikovsky, Physica B 308–310 (2001) 462.
[8] S. Roorda, W.C. Sinke, J.M. Poate, D.C. Jacobson, S. Dierker, B.S. Dennis, D.J. Eaglesham, F. Spaepen, P. Fuoss, Phys. Rev. B 44 (1991) 3702.
[9] S. Roorda, S. Doorn, W.C. Sinke, P.M.L.O. Scholte, E. van Loenen, Phys. Rev. Lett. 62 (1989) 1880.
[10] S.L. Lai, J.Y. Guo, V. Petrova, G. Ramanath, L.H. Allen, Phys. Rev. Lett. 77 (1996) 99.
[11] Microchem Corp. Lift-off Resist Data Sheet, 2002. http://www.microchem.com/products/pdf/lor_data_sheet.pdf.
[12] M. Zhang, M.Yu. Efremov, F. Schiettekatte, E.A. Olson, A.T. Kwan, S.L. Lai, T. Wisleder, J.E. Greene, L.H. Allen, Phys. Rev. B 62 (2000) 10548.
[13] M.Yu. Efremov, F. Schiettekatte, M. Zhang, E.A. Olson, A.T. Kwan, R.S. Berry, L.H. Allen, Phys. Rev. Lett. 85 (2000) 3560.
[14] M.Yu. Efremov, E.A. Olson, M. Zhang, Z. Zhang, L.H. Allen, Phys. Rev. Lett. 91 (2003) 085703.
[15] R. Karmouch, J.-F. Mercure, Y. Anahory, F. Schiettekatte, Appl. Phys. Lett. 86 (2005) 031912.
[16] J.-F. Mercure, R. Karmouch, Y. Anahory, S. Roorda, F. Schiettekatte, Physica B 340–342 (2003) 622.
[17] National Instruments Corporation, Application Note 046, 2003.
[18] M.Yu. Efremov, E.A. Olson, M. Zhang, S.L. Lai, F. Schiettekatte, Z.S. Zhang, L.H. Allen, Thermochim. Acta 412 (2004) 13.
[19] M.Yu. Efremov, E.A. Olson, M. Zhang, F. Schiettekatte, Zishu Zhang, L.H. Allen, Rev. Sci. Instrum. 75 (2004) 179.
[20] J.F. Mercure, Relaxation du silicium amorphe étudiée par nanocalorimetry, M.Sc. Thesis, Université de Montréal, 2005.
[21] J.F. Ziegler, J.P. Biersack, U. Littmark, The Stopping and Range of Ions in Solids, Pergamon Press, 1985.
[22] M.-J. Caturla, T. Diaz de la Rubia, L.A. Marques, G.H. Gilmer, Phys. Rev. B 54 (1996) 16683.
[23] K. Nordlund, M. Ghaly, R.S. Averback, M. Caturla, T. Diaz de la Rubia, J. Tarus Phys. Rev. B 57 (1998) 7556.
[24] S.E. Donnelly, R.C. Birtcher, V.M. Vishnyakov, G. Carter, Appl. Phys. Lett. 82 (2003) 1860.
[25] R. Taillefer, P. Desjardins, F. Schiettekatte, A finite element model of ultra-sensitive thin film calorimeters for the study of size-dependent thermodynamical properties of materials at the nanoscale, in: Proceedings of the First Northeast Workshop on Circuits and Systems, 2003.
[26] A. Jacquot, W.L. Liu, G. Chen, J.- P. Fleurial, A. Dauscher, B. Lenoir, Figure-of-merit and emissivity measurement of fine-grained polycrystalline silicon films, in: Proceedings of the 21st International Conference on Thermoelectrics, 26–29 August 2002, Long Beach, USA, pp. 118–121.
[27] S. Uma, A.D. McConnell, M. Asheghi, K. Kurabayashi, K.E. Goodson, Int. J. Thermophys. 22 (2001) 605.